Electronic supplementary information

Tailoring bismuth defects in Bi_2WO_6 nanosheets for photocatalytic C–H activation

Xinye Li,[a,b,c, 1] Luteng Luo,[a, 1] Hele Guo,[c] Bo Weng,[*c,d,e] Li Sun,[f] Gangamallaiah Velpula,[f] Imran Aslam,[c] Maarten B. J. Roeffaers,[c] Qinghua Chen,[a,b] Lingxing Zeng,[*a,b] Min-Quan Yang[b] and Qingrong Qian[*a,b]

[a] Engineering Research Center of Polymer Green Recycling of Ministry of Education, College of Environmental Science and Engineering, Fujian Normal University, Fuzhou, Fujian 350007, China.

[b] Fujian Key Laboratory of Pollution Control & Resource Reuse, Fuzhou, Fujian 350007, China.

[c] cMACS, Department of Microbial and Molecular Systems, KU Leuven, Celestijnenlaan 200F, 3001 Leuven, Belgium.

[d] CAS Key Laboratory of Urban Pollutant Conversion, Institute of Urban Environment Chinese Academy of Sciences, 1799 Jimei Road, Xiamen 361021, China

[e] University of Chinese Academy of Sciences, 19A Yuquan Road, Beijing 100049, China

[f] Division of Molecular Imaging and Photonics, Department of Chemistry, KU Leuven, Celestijnenlaan 200F, 3001 Leuven, Belgium.

[1] These authors contributed equally to this work.

[*]Corresponding authors:

Email: bweng@iue.ac.cn; zenglingxing@fjnu.edu.cn; qrqian@fjnu.edu.cn

Experimental

1.1. Synthesis of bulk-BT nanosheets

0.5 mmol $Bi(NO_3)_3{\cdot}5H_2O$, 0.5 mmol $Na_2WO_4 \cdot 2H_2O$ and 0.1 g CTAB were initially dissolved in 80 ml DI water under magnetic stirring at room temperature. After being stirred for 30 min, the suspension was transferred to a 100 mL Teflon-lined autoclave and subsequently heated at 120 °C for 24 h to achieve the bulk-BT nanosheets.

1.2. Synthesis of ultrathin BT-48 nanosheets

0.5 g bulk-BT nanosheets were dispersed in 70 mL 1 M HNO_3 solution under ultrasound for 30 min. Then above dispersions were stirring for 1.5h. Subsequently, the above suspension was added into a 100 mL Teflon-lined autoclave and heated at 120 °C for 48h. The precipitate was collected and washed with deionized water several times and dried at 80 °C.

1.3 Characterization

Transmission electron microscopy (TEM) images of samples were obtained using a probe-lens corrected JEOL ARM200F operating at 200 kV, equipped with a cold-field emission source and Centurion EDX detector. AFM images were recorded using Agilent 5,500 AFM (Agilent Technologies, USA). X-ray diffractometry (XRD) measurements were performed on a Stoe X-ray diffractometer using Cu Kα1 radiation (λ = 1.5406 Å). Raman scattering experiments were performed on a homemade system using a TriVistaTM Spectrometer System (triple grating; 900, 900 and 1800 gg/mm) with a N2-cooled CCD detector from Princeton Instruments. Electron paramagnetic resonance (EPR) measurement was recorded using an MS 5000. X-ray photoelectron spectroscopy (XPS) data were recorded on a VG ESCALAB XPS System with a monochromatized Al Ka X-ray source (15 kV, 200 W 500 um pass energy = 20 eV). All binding energies were referenced to the C1s peak at 284.6 eV of surface adventitious carbon. Micromeritics ASAP2010 equipment was used to obtain the nitrogen adsorption-desorption isotherms and the Brunauer-Emmett-Teller (BET) surface areas at 77 K. The powders were degassed at 413 K to remove all surface-adsorbed contaminants before measurements. CO_2 adsorption isotherms measurements for all the synthetic samples were carried out using an automatic microporous physical and chemical gas adsorption analyzer (ASAP 2020 M PLUS). An ultraviolet–visible spectrophotometer (UV–vis, Lambda-950) was employed to obtain the optical properties of the samples by UV–vis diffuse reflectance spectroscopy (DRS) in the wavelength 300–800 nm with 1 nm increment, where $BaSO_4$ and black carbon were used as the references. The electrochemical analysis was carried out with an electrochemical workstation (Chenhua CHI660) in a conventional three-electrode cell. The reference electrode was an Ag/AgCl electrode, and a platinum sheet was used as the counter electrode. The electrolyte is aqueous solution of 0.01 M $K_3[Fe(CN)_6]$/ $K_4[Fe(CN)_6]$(1:1).

1.4 Photocatalytic activity measurements.

All photocatalytic reactions were conducted in a 20 mL quartz reactor and with a magnetic stirring rod (500 rpm). The specific procedure was as follows: 15 mg photocatalyst, and 2.5 mL toluene prior to being saturated with molecular oxygen were loaded into the reactor and then the whole system was sealed up. The mixture was irradiated with a 150 W Xe lamp with an AM 1.5G filter or 420 nm cut-off filter to simulate the solar light spectrum. After irradiation of 4 h, the suspension was centrifuged at 10000 rpm for 10 min and the liquid was analyzed by Shimadzu GC-2010. Control photoactivity experiments with different radical scavengers, ammonium oxalate, potassium persulfate, and 1,4-benzoquinone as scavengers for photogenerated holes, photogenerated electrons, and superoxide radical specials, respectively, were performed under similar reaction conditions.

1.5 Measurement of H_2O_2.

0.05 mL of 0.01 mol L^{-1} ammonium molybdate aqueous solution and 2 mL of 0.1 mol L^{-1} potassium iodide aqueous solution were added to 1 mL obtained solution, and kept for 30 min. The H_2O_2 molecules reacted with iodide anions (I^-) to produce triiodide anions (I_3^-). The amount of I_3^- was determined by means of UV-vis spectroscopy on the basis of the absorbance at 325 nm. The background is prepared by the mixture of ammonium molybdate aqueous solution and potassium iodide aqueous solution. The background + H_2O_2 is prepared by background adding 10 μl H_2O_2 to the solution.

1.6 Density functional theory (DFT) calculation details.

In this study, we performed density functional theory (DFT) calculations using the Vienna ab initio simulation package[S1] (VASP) with the projector augmented wave[S2] (PAW) and generalized gradient approximations[S3] (GGA) of Perdew–Burke–Ernzerhof (PBE) pseudopotentials.[S4] For the simulation of defect Bi_2WO_6 nanosheet research, a 2 x 2 x 1 supercell was established. A Bi atom is removed from the supercell to construct a BT-48 model, with all the other parameters remained unchanged. The convergence criteria for energy and force were set as 10^{-6} eV and 0.03 eV/Å, respectively. and the cutoff energy for the plane wave was 500 eV. The optimized lattice constant for the double-layer Bi_2WO_6 nanosheet primitive cell was 5.50 Å x 5.80 Å. And a 20 Å vacuum layer was added to avoid inter-layer interactions.

1.7 The chemical equations of the toluene oxidation reaction over BT-48 are defined as follows:

$$\text{BT-48} + h\nu \rightarrow h^+ + e^- \quad (1)$$

$$\text{R-CH}_3 + h^+ \rightarrow \text{R-CH}_2^* + H^+ \quad (2)$$

$$O_2 + e^- \rightarrow \cdot O_2^- \quad (3)$$

$$\text{R-CH}_2^* + \cdot O_2^- \rightarrow \text{R-CHO} + OH^- \quad (4)$$

$$OH^- + h^+ \rightarrow \cdot OH \quad (5)$$

$$\text{R-CH}_2^* + \cdot OH \rightarrow \text{R-CH}_2OH \quad (6)$$

$$\text{R-CH}_2OH + h^+ + \cdot OH \rightarrow \text{R-CHO} + H_2O + H^+ \quad (7)$$

$$\text{R-CH}_2OH + h^+ \rightarrow \text{R-CH}_2O^* + H^+ \quad (8)$$

$$\cdot O_2^- + H^+ \rightarrow \cdot OOH \quad (9)$$

$$\text{R-CH}_2O^* + \cdot OOH \rightarrow \text{R-CHO} + H_2O_2 \quad (10)$$

References

[S1] J. Hafner, *J. Comput. Chem.*, 2008, **29 (13)**, 2044-2078.

[S2] J.P. Perdew, Y. Wang, *Phys. Rev. B,* 1992, **45 (23)**,13244-13249.

[S3] G. Kresse, J. Hafner, Phys. Rev. B, 1993, **48 (17)**, 13115-13118.

[S4] J.P. Perdew, K. Burke, Y. Wang, Phy. Rev. B, 1996, **54 (23)**,16533-16539.

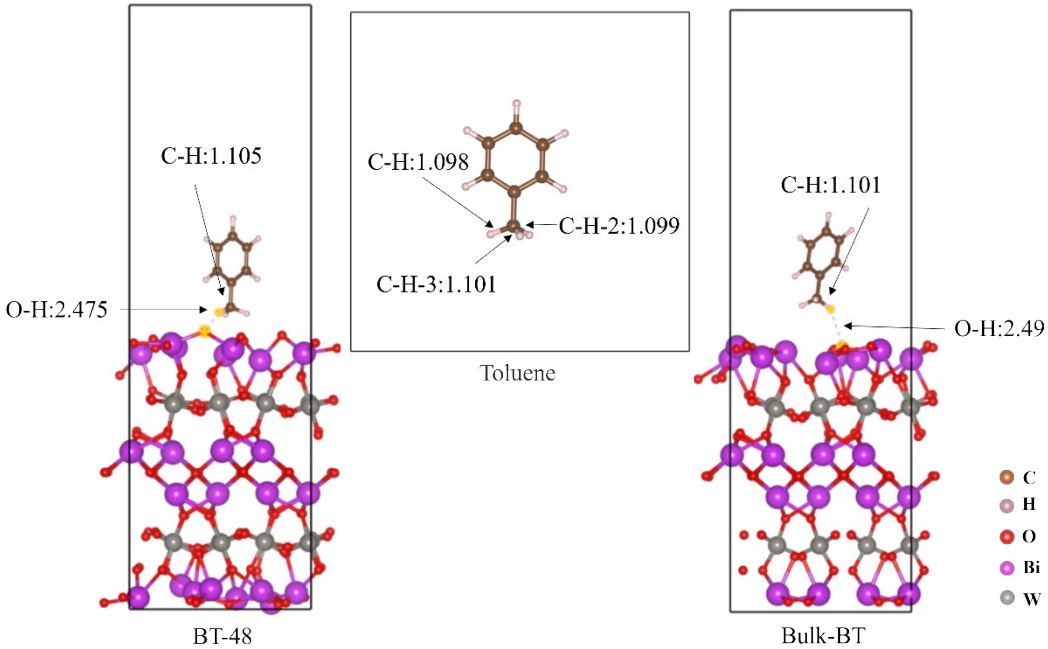

Fig. S1 DFT-derived optimized structures and the adsorption of toluene on Bulk-BT and BT-48.

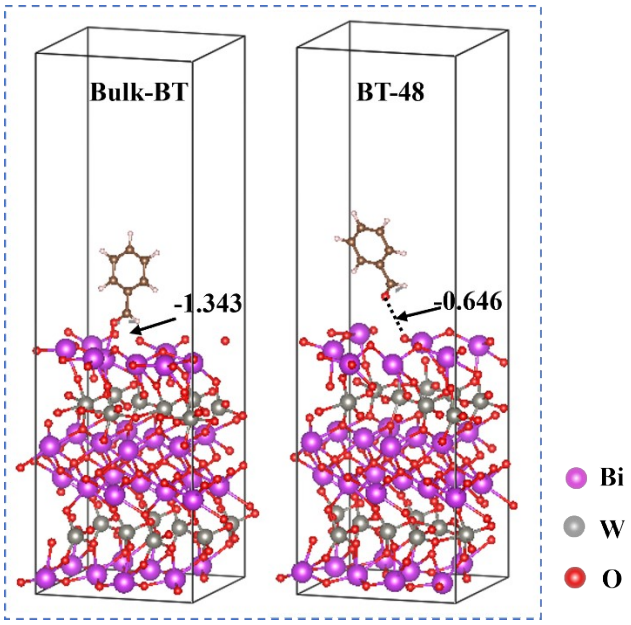

Fig. S2 DFT-derived optimized structures and the adsorption of benzaldehyde on Bulk-BT and BT-48.

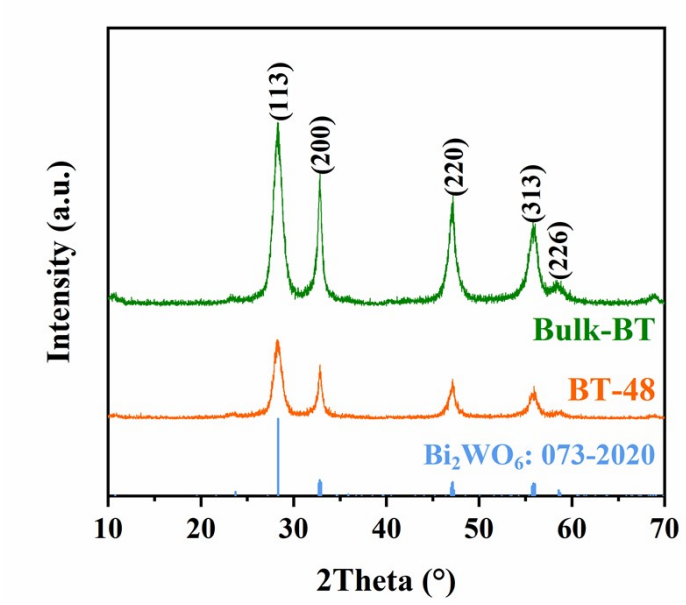

Fig. S3 XRD patterns of Bulk-BT and BT-48 samples.

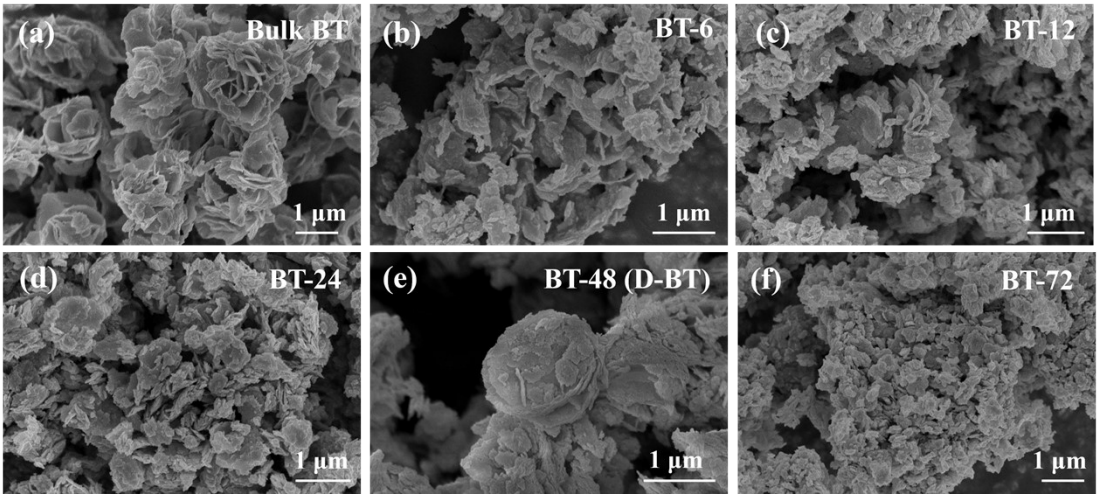

Fig. S4 SEM images of all Bi_2WO_6 samples.

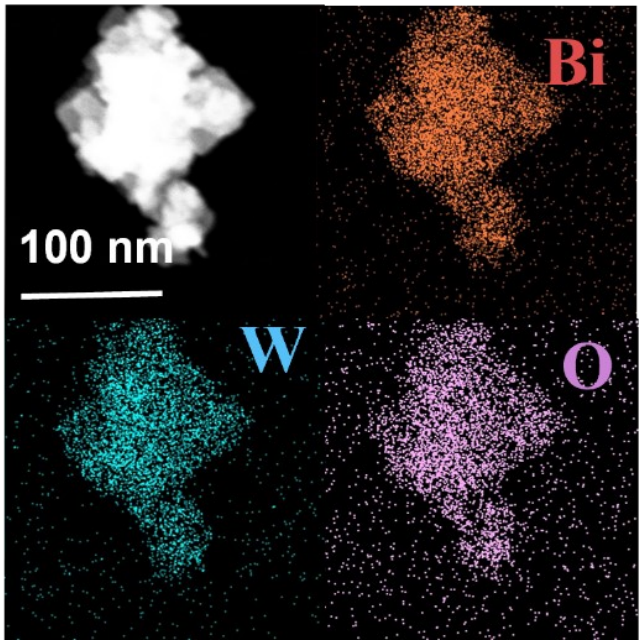

Fig. S5 EDS spectra of BT-48 sample.

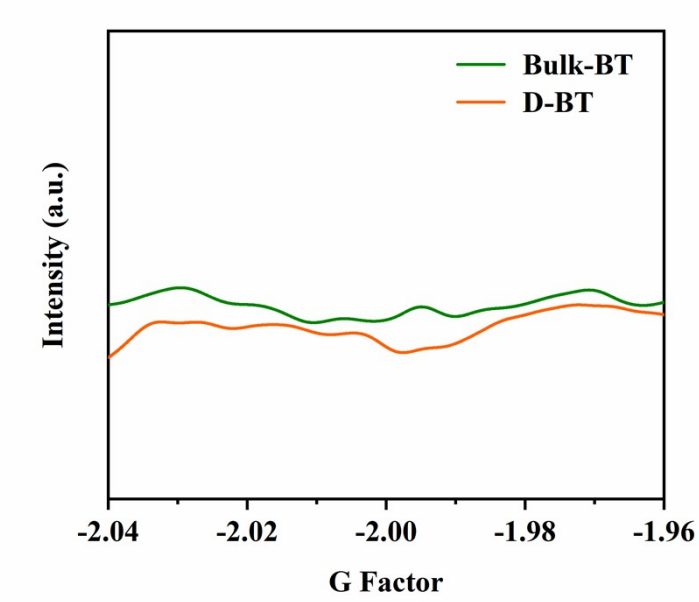

Fig. S6 EPR spectra of Bulk-BT and BT-48 samples.

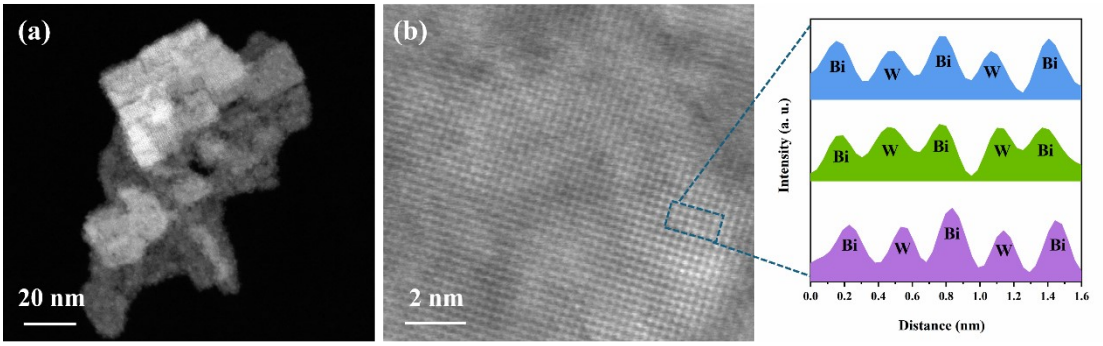

Fig. S7 (a) TEM image, (b) HAADF-STEM image with Intensity along the blue box of Bulk-BT sample.

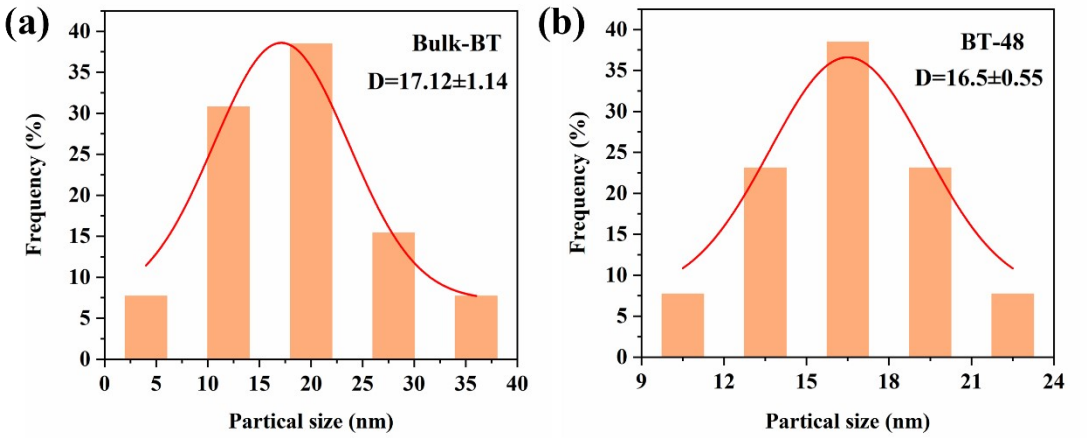

Fig. S8 (a) The size distribution of the Bulk-BT, counted and calculated from **Fig. S7a** (b) The size distribution of the BT-48 nanosheets, counted and calculated from **Fig. 2a**.

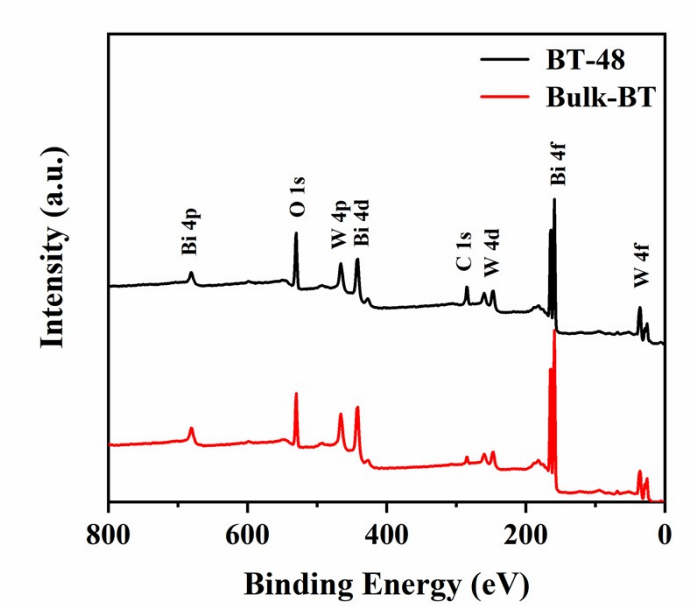

Fig. S9 XPS survey spectra of Bulk-BT and BT-48 samples.

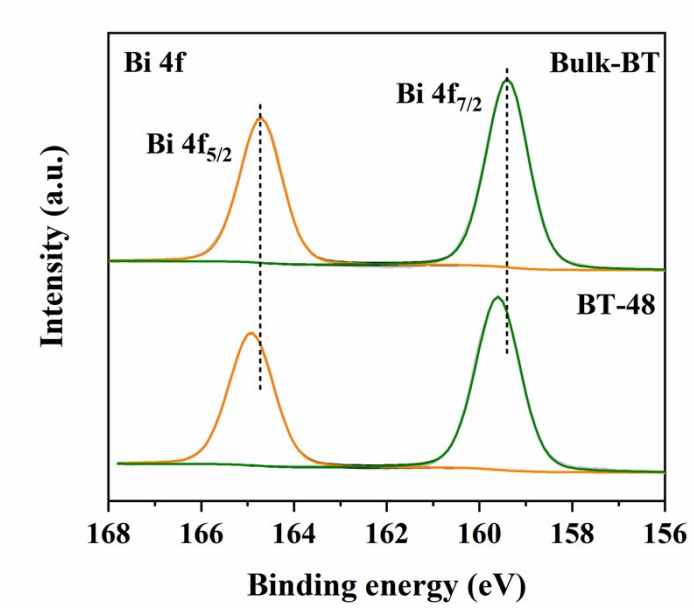

Fig. S10 XPS spectra of Bulk-BT and BT-48 samples: Bi 4f.

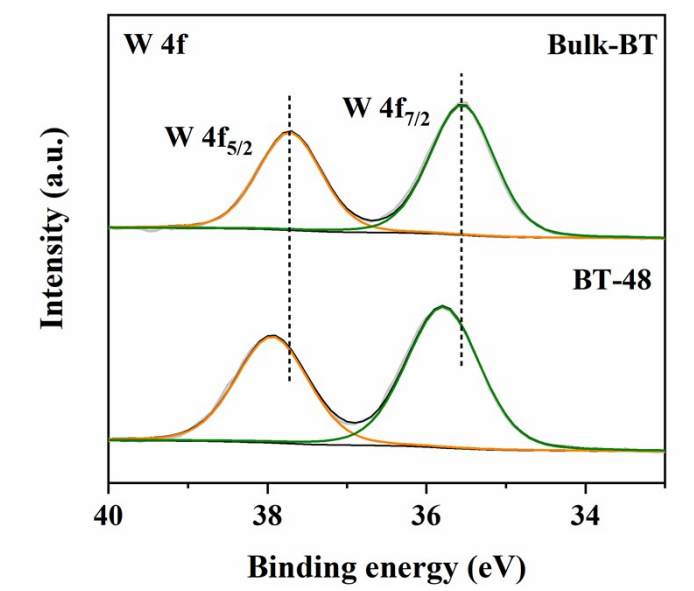

Fig. S11 XPS spectra of Bulk-BT and BT-48 samples: W 4f.

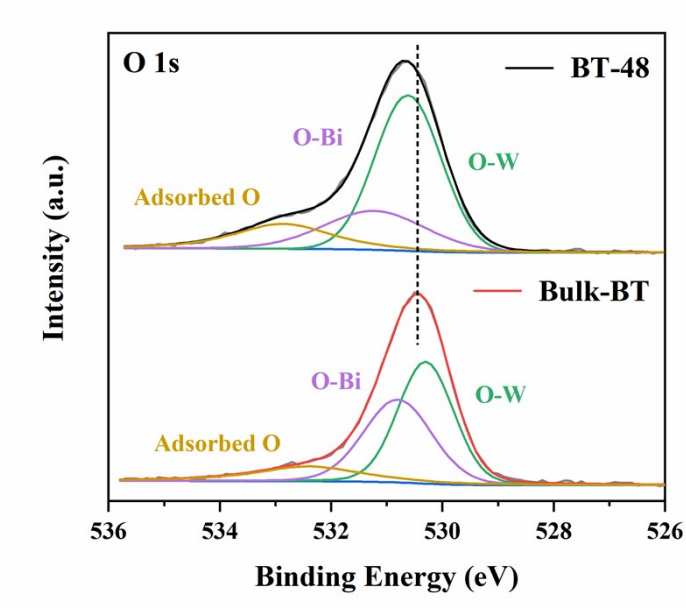

Fig. S12 XPS spectra of Bulk-BT and BT-48 samples: O 1s.

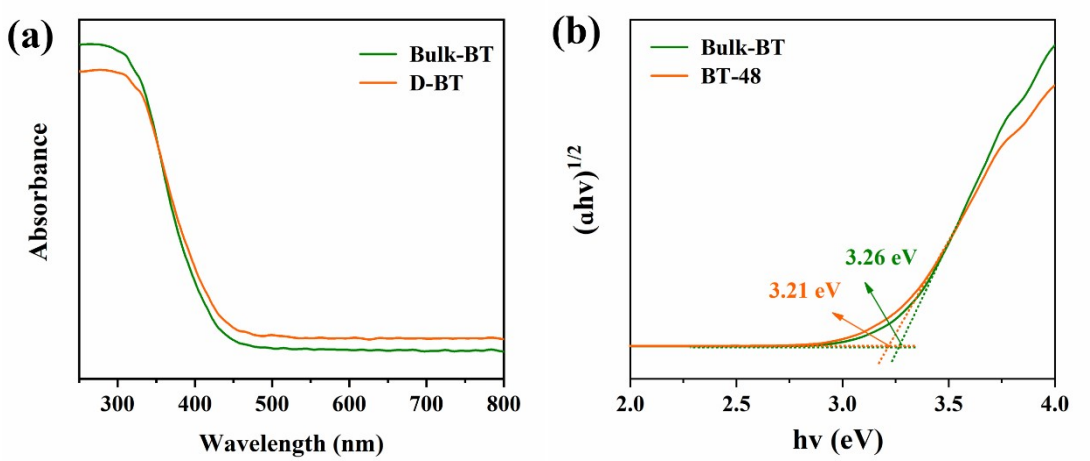

Fig. S13 UV-Vis absorption (a) and Tauc plots (b) of Bulk-BT and BT-48 samples.

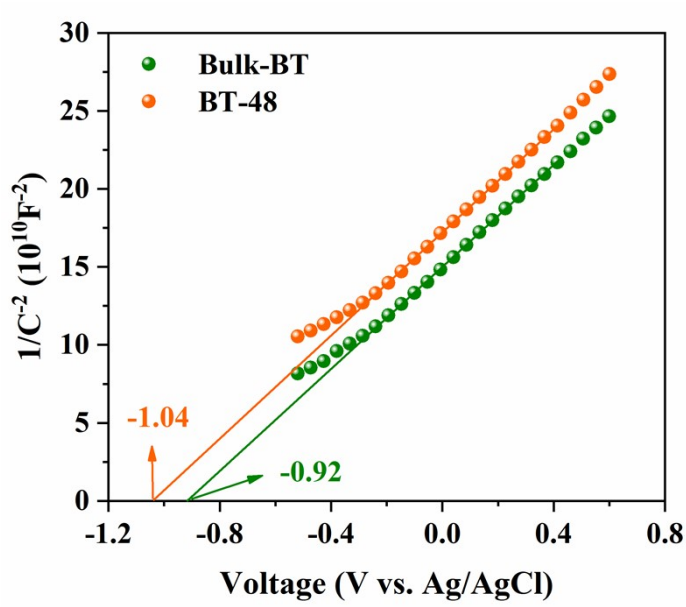

Fig. S14 Mott−Schottky plots of Bulk-BT and BT-48 samples.

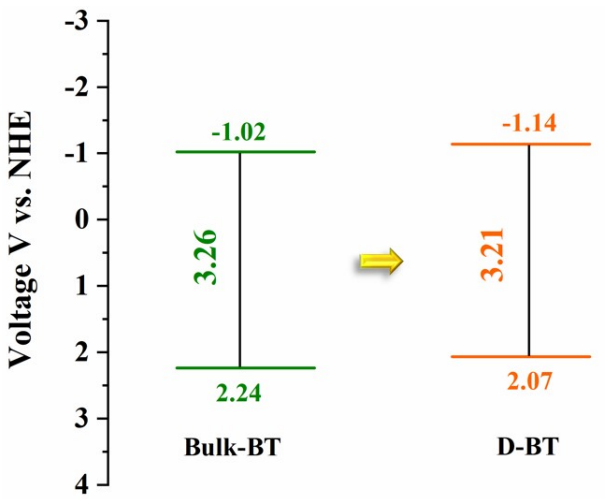

Fig. S15 Schematics of energy band alignment of Bulk-BT and BT-48 samples.

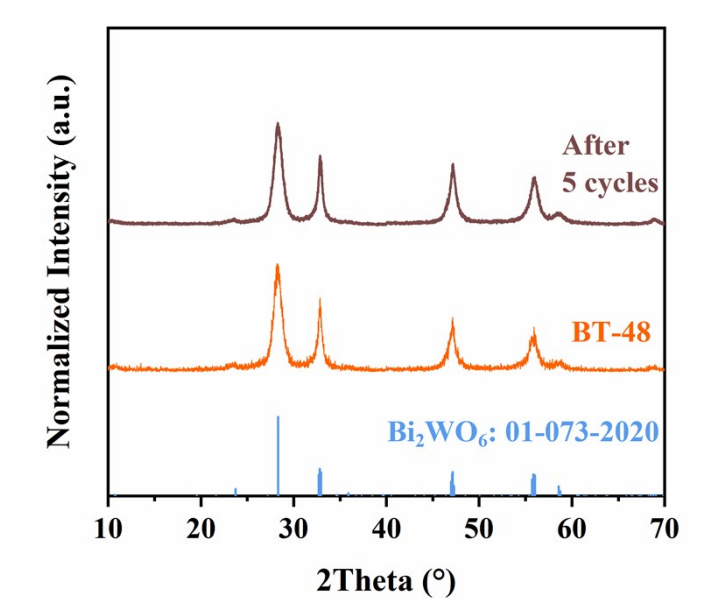

Fig. S16 XRD patterns of BT-48 before and after 5 cycles.

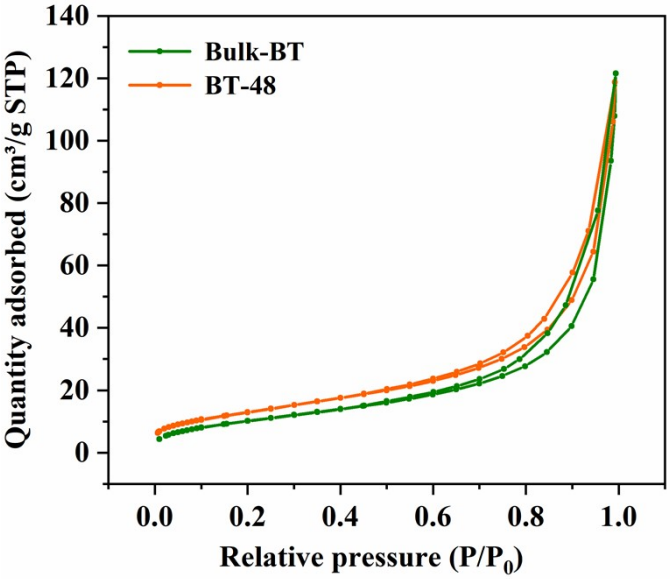

Fig. S17 N_2 physisorption of Bulk-BT and BT-48 samples.

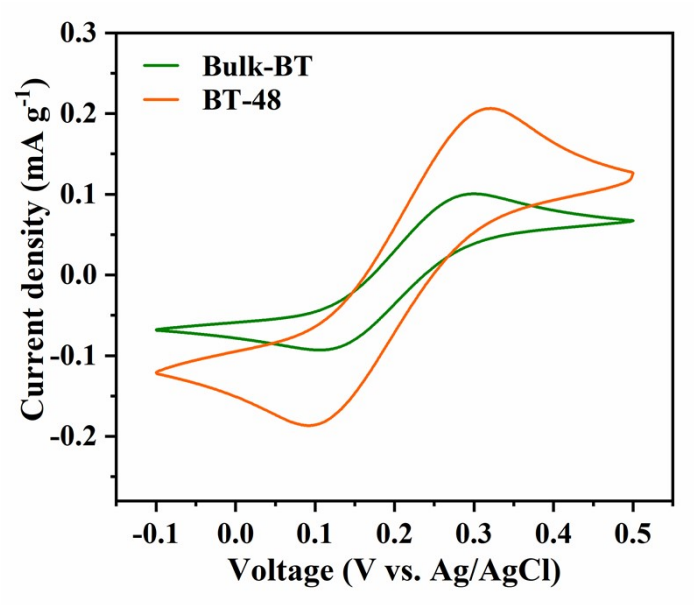

Fig. S18 Cyclic voltammetry curves of Bulk-BT and BT-48 samples.

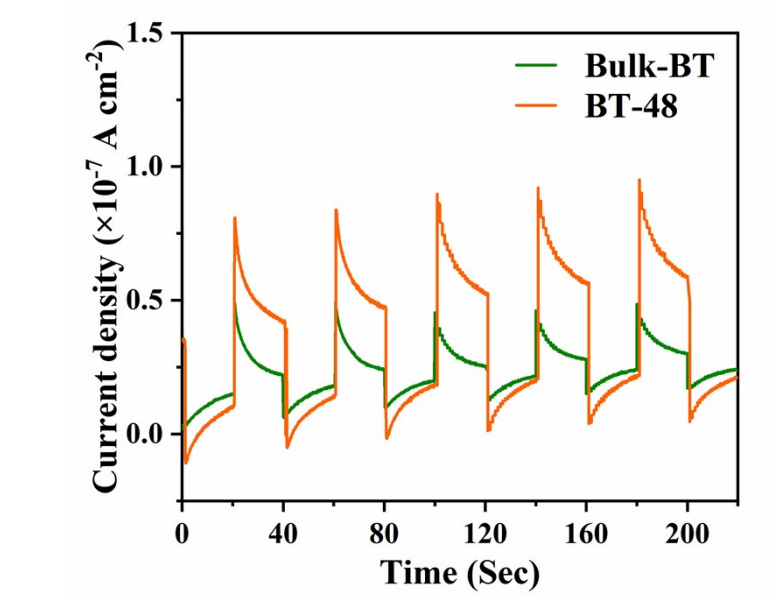

Fig. S19 Photocurrent responses of Bulk-BT and BT-48 samples.

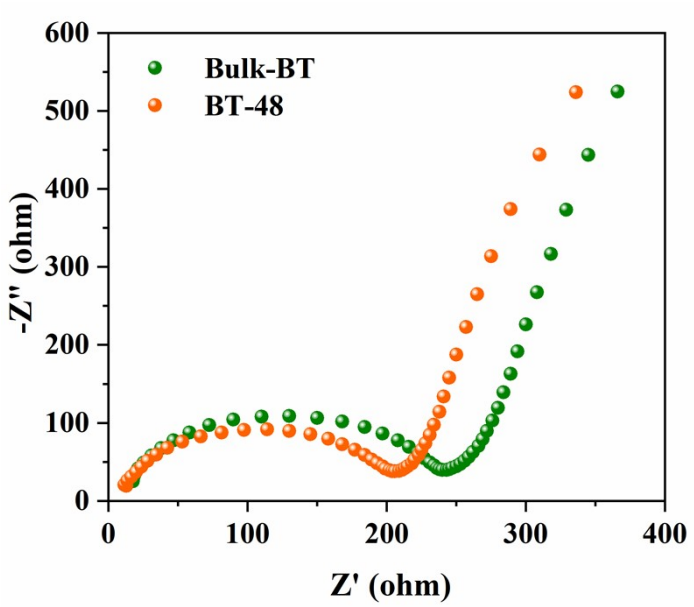

Fig. S20 Electrochemical impedance spectroscopy spectra of Bulk-BT and BT-48 samples.

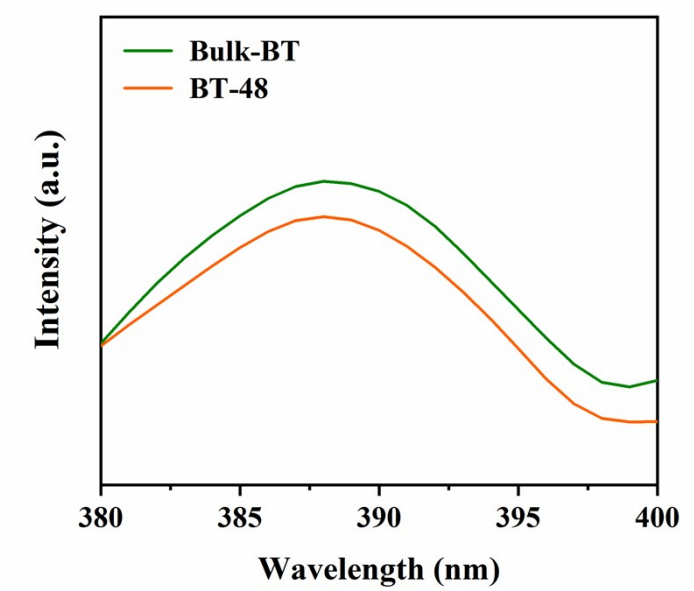

Fig. S21 PL spectra of Bulk-BT and BT-48 samples.

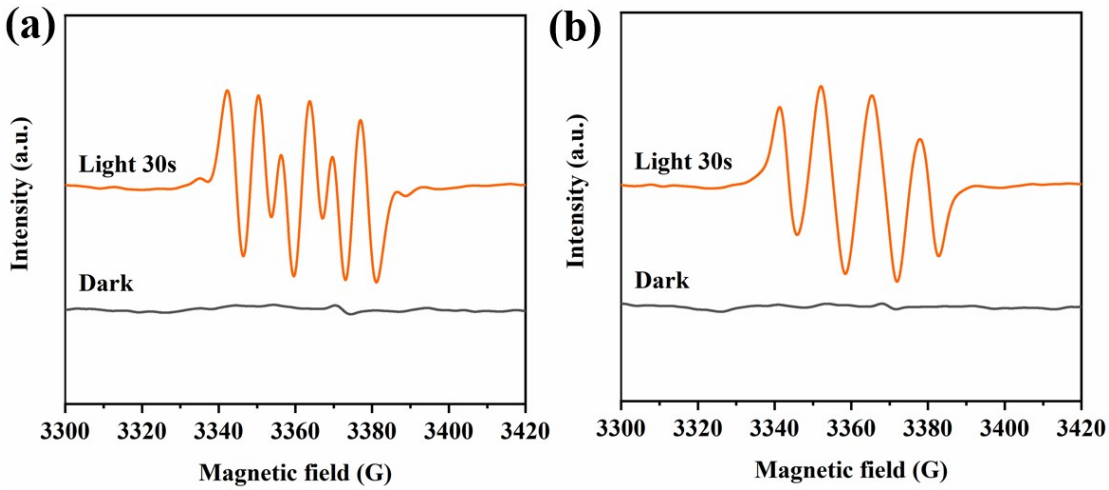

Fig. S22 ESR spectra air for the detection of (a) $\cdot O_2^-$ and (b) ·OH in BT-48 sample.

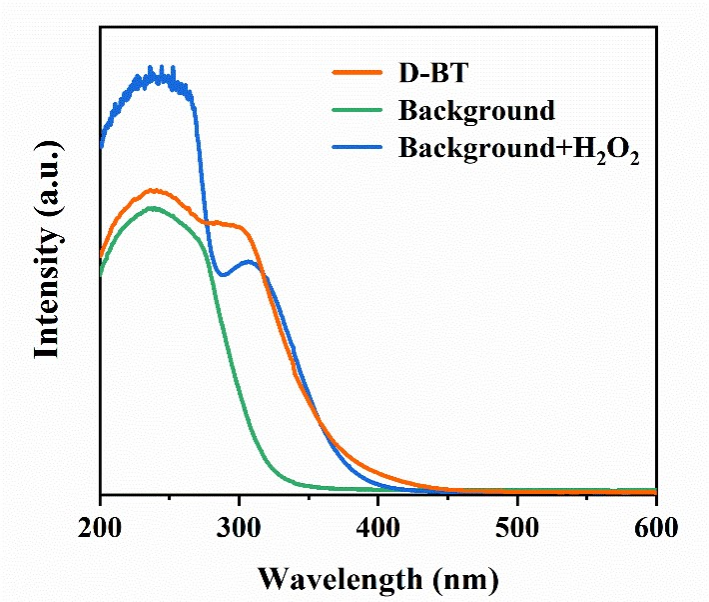

Fig. S23 UV–Vis spectra of hydrogen peroxide production over BT-48 sample.

Table S1 Surface atomic concentration of Bulk-BT and BT-48 samples calculated from XPS.

Sample	Element content (mol%)			
	Bi	W	Bi/W	theoretical Bi/W
BT-48	11.93%	6.7%	1.78	2
Bulk-BT	15.82%	7.52%	2.1	2

Table S2 Comparison of the catalytic activity for benzaldehyde formulation rate over Bi_2WO_6-based photocatalysts.

References

Catalysts	Production rate (μmol g^{-1} h^{-1})	Light source	atmosphere	Stability (h)	Selectively (%)	References
V_{Bi}-Bi_2WO_6	6781	Simulated sunlight	O_2	20	96	This work
Pd/Bi_2WO_6	1140	visible-light	O_2	35	92	S1
TiO_2/Bi_2MoO_6	1037	visible-light	O_2	15	97	S2
Fe/Bi_2WO_6	1304	visible-light	O_2	25	97	S3
$Bi_2W_{0.3}Mo_{0.7}O_6$	1663	visible-light	O_2	20	91	S4
Flower-like Bi_2WO_6	464	visible-light	O_2	25	96	S5
4%Pt/2%Ta-Bi_2WO_6	675	visible-light	Ar	30	99	S6
Bi_2WO_6	763	simulated sunlight	O_2	60	100	S7
Bi_2WO_x	2162	visible-light	O_2	30	100	S8
V_W-Bi_2WO_6	3474	simulated sunlight	O_2	40	>99	S9
Bi_2WO_6/ZnS	1000	visible-light	Air	30	>99	S10
Bi_2WO_6/CdS	2200	visible-light	Air	30	>99	S10

[S1] B. Yuan, B. Zhang, Z. Wang, S. Lu, J. Li, Y. Liu, C. Li, *Chin. J. Catal.*, 2017, **38**, 440-446.

[S2] L. N. Song, F. Ding, Y. K. Yang, D. Ding, L. Chen, C. T. Au and S. F. Yin, *ACS Sustain. Chem. Eng.*, 2018, **6**, 17044-17050.

[S3] X. X. Deng, S. Tian, Z. M. Chai, Z. J. Bai, Y. X. Tan, L. Chen, J. K. Guo, S. Shen, M. Q. Cai, C. T. Au and S. F. Yin, *Ind. Eng. Chem. Res.*, 2020, **59**, 13528-13538.

[S4] K. Zhang, H. Chen, Y. Liu, J. Deng, L. Jing, A. Rastegarpanah, W. Pei, Z. Han and H. Dai, *Appl. Catal. B: Environ.*, 2022, **315**, 121545.

[S5] Y. Liu, L. Chen, Q. Yuan, J. He, C. T. Au and S. F. Yin, *Chem. Commun.*, 2016, **52**, 1274-1277.

[S6] Z. Shen, Y. Hu, Q. Pan, C. Huang, B. Zhu, W. Xia, H. Wang, J. Yue, M. Muhler, G. Zhao, X. Wang and X. Huang, *Appl. Surf. Sci.*, 2022, **571**, 151370.
[S7] Q. Gu, K. Zhang, P. Jiang, Y. Shen, Y. Leng, P. Zhang and P. T. Wai, *Mol. Catal.*, 2021, **515**, 111932.
[S8] X. Cao, Z. Chen, R. Lin, W. C. Cheong, S. Liu, J. Zhang, Q. Peng, C. Chen, T. Han, X. Tong, Y. Wang, R. Shen, W. Zhu, D. Wang and Y. Li, , *Nat. Catal.*, 2018, **1**, 704-710.
[S9] H. Huang, C. Zhou, X. Jiao, H. Yuan, J. Zhao, C. He, J. Hofkens, M. B. J. Roeffaers, J. Long and J. A. Steele, *ACS Catal.*, 2019, **10**, 1439-1443.
[S10] E. Safaei and S. Mohebbi, *J. Photochem. Photobiol. A Chem.*, 2019, **371**, 173-181.